toxins

MDPI

Article

Engineering Gain-of-Function Analogues of the Spider Venom Peptide HNTX-I, A Potent Blocker of the hNa$_V$1.7 Sodium Channel

Yunxiao Zhang †, Qiuchu Yang †, Qingfeng Zhang, Dezheng Peng, Minzhi Chen, Songping Liang, Xi Zhou * and Zhonghua Liu *

The National & Local Joint Engineering Laboratory of Animal Peptide Drug Development, College of Life Sciences, Hunan Normal University, Changsha 410081, Hunan, China; Zhangyx0954@163.com (Y.Z.); QQQQiuchu@126.com (Q.Y.); feng122436ab@126.com (Q.Z.); pdz920217@sina.com (D.P.); chenmz@hunnu.edu.cn (M.C.); liangsp@hunnu.edu.cn (S.L.)

* Correspondence: xizh@hunnu.edu.cn (X.Z.); liuzh@hunnu.edu.cn (Z.L.); Tel: +86-731-8887-2556 (Z.L.); Fax: +86-731-8886-1304 (Z.L.)

† These authors contributed equally to this work.

Received: 3 August 2018; Accepted: 31 August 2018; Published: 4 September 2018

Abstract: Pain is a medical condition that interferes with normal human life and work and reduces human well-being worldwide. Human voltage-gated sodium channel NaV1.7 (hNaV1.7) is a compelling target that plays a key role in human pain signaling. The 33-residue peptide μ-TRTX-Hhn2b (HNTX-I), a member of Na$_V$-targeting spider toxin (NaSpTx) family 1, has shown negligible activity on mammalian voltage-gated sodium channels (VGSCs), including the hNa$_V$1.7 channel. We engineered analogues of HNTX-I based on sequence conservation in NaSpTx family 1. Substitution of Asn for Ser at position 23 or Asp for His at position 26 conferred potent activity against hNa$_V$1.7. Moreover, multiple site mutations combined together afforded improvements in potency. Ultimately, we generated an analogue E1G–N23S–D26H–L32W with >300-fold improved potency compared with wild-type HNTX-I on hNa$_V$1.7 (IC$_{50}$ 0.036 ± 0.007 μM). Structural simulation suggested that the charged surface and the hydrophobic surface of the modified peptide are responsible for binding affinity to the hNa$_V$1.7 channel, while variable residues may determine pharmacological specificity. Therefore, this study provides a profile for drug design targeting the hNa$_V$1.7 channel.

Keywords: voltage-gated sodium channels; Na$_V$1.7; spider venom; toxin; HNTX-I; engineering

Key Contribution: This study engineered a gain-of-function analogue of HNTX-I with great potency on hNa$_V$1.7 based on sequence conservation in the family. It provides a profile for peptide drug design.

1. Introduction

Pain treatment causes significant health concerns and economic burdens for affected families and for society [1–3]. Currently available drugs have safety and tolerability limitations and are often ineffective or suboptimally used [4–6]. There is therefore a critical unmet medical need to discover novel potential analgesia candidates, as well as to improve currently available therapies for severe and chronic pain [7].

Human Na$_V$1.7 (hNa$_V$1.7) has been identified as an important channel playing a crucial role in human pain signaling [8]. It is preferentially expressed in peripheral neurons, including peripheral somatic and visceral sensory neurons within the dorsal-root ganglia, sympathetic ganglion neurons,

myenteric neurons and olfactory–sensory neurons [9,10]. In humans, gain-of-function mutations of $hNa_V1.7$ lead to severe neuropathic pain, such as inherited erythromelalgia (IEM) [11–13], paroxysmal extreme pain disorder (PEPD) [14,15] and idiopathic small-fiber neuropathy (SFN) [16], while loss-of-function mutations cause congenital insensitivity to pain (CIP) [17]. Based on the results of validated and compelling genetic studies, $hNa_V1.7$ has become an outstanding target for developing new therapies for pain [18].

Natural peptide toxins from animal venom have been an invaluable and original source of novel, selective and potent modulators targeting ion channels implicated in pain signaling pathways [19]. Indeed, some peptide toxins derived from animal venoms inhibit the $hNa_V1.7$ channel and exhibit remarkable analgesia. Spider venom–derived peptide toxins can be divided into 12 distinct families that target Na_V channels based on primary structure and cysteine scaffold. Peptides in Na_V-targeting spider toxin (NaSpTx) family 1 contain 33–35 amino acid residues, with 3 disulfide bridges forming an inhibitory cystine-knot (ICK) motif., Through the alignment and structural analysis of conserved sequences, it is possible to rationally design novel peptides that are likely to inhibit the $Na_V1.7$ channel.

Previously, we reported the identification of 33-residue peptide μ-TRTX-Hhn2b (HNTX-I), a member of NaSpTx family 1, from the venom of the spider *Selenocosmia hainana*. Although the amino acid sequence of this family is highly conserved, HNTX-I has shown weak affinity on insect sodium channels and no effect on mammalian voltage-gated sodium channels (VGSCs), unlike the majority of peptide toxins in NaSpTx family 1 [20]. In this study, we used HNTX-I as a framework and engineered analogues of it based on sequence conservation in the family. Ultimately, we engineered a gain-of-function analogue of HNTX-I: E1G-N23S-D26H-L32W, a potent blocker of the $hNa_V1.7$ channel with an IC_{50} value of 0.036 ± 0.007 μM. Our data define the motif $X_1X_2SWCKX_3$ as critical for suppressing the $hNa_V1.7$ channel.

2. Results

2.1. Sequence Alignment of HNTX-I in NaSpTx Family 1

Figure 1A shows the amino acid sequence alignment of peptides in NaSpTx family 1. Conserved cystine residues are highlighted in red. These peptides form an ICK motif that is typically resistant to extremes of pH, organic solvents, high temperatures and proteases [21]. A sequence logo for this alignment is displayed in Figure 1B. The overall height of the stack indicates sequence conservation at that position, while the height of the letter within the stack indicates the relative frequency of each amino acid at that position. Proline at position 12, tryptophan at position 31 and lysine at position 33 are not buried, indicating that residues here appear to be critical for peptide activity. Positions that are partially or completely buried tend to be populated by the corresponding residues. For example, serine is more popular in position 26, as is aspartic acid in position 29. In particular, the serine in position 26 has been demonstrated to be important for activity [22,23], which validates the feasibility of modifying peptide activity according to sequence conservation.

A

Toxins	Sequences	Targets
μ-TRTX-Hhn2b	-ECKGFGKSCVPGKNECCS--GYACNSRDKWCKVLL-	Insect para/tipE
μ-TRTX-Hhn1a	-ECLGFGKGCNPSNDQCCKSANLVCSRKHRWCKYEI-	Na_v
μ-TRTX-Hhn1b	-ECLGFGKGCNPSNDQCCKSSNLVCSRKHRWCKYEI-	Na_v
μ-TRTX-Hhn2a	-GCKGFGDSCTPGKNECCP--NYACSSKHKWCKVYL-	Na_v
μ-TRTX-Hs2a	-ECLEIFKACNPSNDQCCKSSKLVCSRKTRWCKYQI-	Na_v
β-TRTX-Ps1a	-DCLGFLWKCNPSNDKCCR-PNLVCSRKDKWCKYQI-	Na_v
β-TRTX-Cd1a	-DCLGWFKSCDPKNDKCCK--NYSCSRRDRWCKYDL-	$Na_v/Ca_v2.2$
β-TRTX-Cm1a	-DCLGWFKSCDPKNDKCCK--NYTCSRRDRWCKYDL-	$Na_v/Ca_v2.2$
β-TRTX-Cm1b	-DCLGWFKSCDPKNDKCCK--NYTCSRRDRWCKYYL-	$Na_v/Ca_v2.2$
κ-TRTX-Gr4a	-DCLGWFKGCDPDNDKCCE--GYKCNRRDKWCKYKLW	Na_v/K_vAP
κ-TRTX-Tb1a	AACLGMFESCDPNNDKCCP--NRECNRKHKWCKYKLW	$K_v4.2$
κ-TRTX-Tb1b	DDCLGMFSSCDPKNDKCCP--NRVCRSRDQWCKYKLW	$K_v4.2$
κ-TRTX-Tb1c	DDCLGMFSSCDPNNDKCCP--NRVCRVRDQWCKYKLW	$K_v4.2$

B

Figure 1. Sequence alignment of peptide toxins in the NaSpTx family 1. (**A**) Alignment of mature toxin sequences in NaSpTx family 1. Cysteines are highlighted in red; (**B**) Sequence logo for alignment in NaSpTx family 1. Residues shown in black are hydrophobic, those shown in red are negatively charged, those shown in blue are positively charged, and those shown in green are polar uncharged. The overall height of the stack indicates the sequence conservation at that position, while the height of letter within the stack indicates the relative frequency of each amino acid.

2.2. *Rational Design of HNTX-I in Consideration of Sequence Conservation*

As mentioned above, we conducted amino acid substitutions at the following positions in HNTX-I. Asparagine in position 23 was mutated to serine (N23S), and aspartic acid in position 26 was mutated to histidine (D26H). In the NaSpTx family 1, a triple mutant of HWTX-IV (E1G, E4G, Y33W–HWTX–IV) showed a great increase of potency against $Na_V1.7$ [24]. Therefore, we mutated glutamic acid in position 1 to glycine (E1G) and leucine in position 32 to tryptophan (L32W) in the hopes of increasing affinity to $Na_V1.7$. However, similar to wild-type HNTX-I, E1G and L32W had negligible activity on $Na_V1.7$ at a concentration of 10 μM (Figure 2A–C). Notably, N23S showed an obvious increase in activity (IC_{50} 0.435 ± 0.072 μM), tenfold higher than previously reported [22]. In addition, D26H conferred $Na_V1.7$-inhibitory activity on HNTX-I with an IC_{50} value of 1.498 ± 0.093 μM. Therefore, N23S and D26H individually contributed to inhibition of $hNa_V1.7$ (Figure 2D and Table 1).

It has been reported that the activity of a combination of mutants is not necessarily better than that of a single mutant [25]. We combined the single mutants described above to see whether activity would increase significantly. As shown in Figure 2D,E and Table 1, N23S–D26H demonstrated an obvious increase in potency (IC_{50} 0.079 ± 0.004 μM) against $hNa_V1.7$, compared with individual mutants. However, the combination of N23S–D26H with E1G (E1G–N23S–D26H) reduced activity (IC_{50} 0.179 ± 0.024 μM), while the mutant into which N23S–D26H and L32W were combined (N23S–D26H–L32W) exhibited activity (IC_{50} 0.071 ± 0.005 μM) close to that of N23S–D26H. We also tried to combine these single mutants together. Ultimately, the mutant E1G–N23S–D26H–L32W caused the greatest increase in activity (IC_{50} 0.036 ± 0.007 μM). The dose–response curves of N23S–D26H, N23S–D26H–L32W and E1G–N23S–D26H–L32W are shown in Figure 2E.

Meanwhile, we also tried to replace arginine in position 25 with the more popular lysine at the same charge. Neither E1G–R25K–D26H (IC_{50} 0.766 ± 0.029 μM) nor E1G–R25K–D26H–L32W (IC_{50} 0.669 ± 0.070 μM) showed stronger activity than did E1G–N23S–D26H–L32W (Figure 2D and Table 1). In summary, we successfully engineered a gain-of-function analogue of HNTX-I with potent inhibitory effect on mammalian sodium channel $hNa_V1.7$ by the method of sequence conservation in the family.

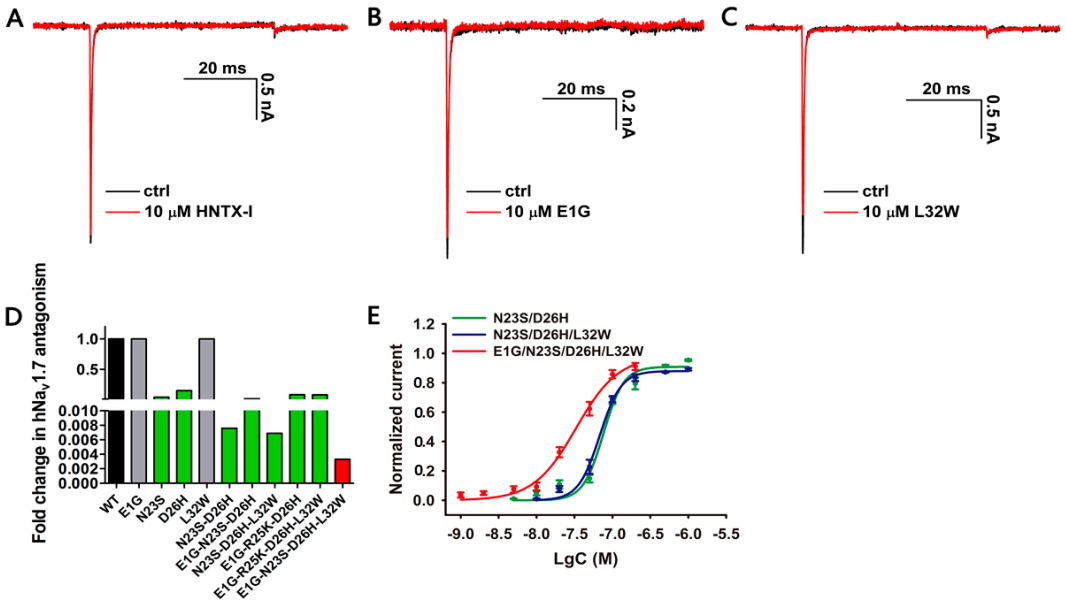

Figure 2. Inhibitory activity of HNTX-I analogues on $Na_V1.7$. (**A**) Representative $Na_V1.7$ current trace before (black) and after (red) addition of 10 μM wild-type HNTX-I; (**B**) Representative $Na_V1.7$ current trace before (black) and after (red) addition of 10 μM E1G; (**C**) Representative $Na_V1.7$ current trace before (black) and after (red) addition of 10 μM L32W; (**D**) Fold change of inhibitory effect of wild-type HNTX-I and HNTX-I analogues on $Na_V1.7$; (**E**) Concentration–response curves of N23S–D26H, N23S–D26H–L32W and E1G–N23S–D26H–L32W analogues assessed by whole-cell patch clamp. Data are mean ± SEM, with n = 3–5 cells per data point.

Table 1. IC_{50} value of HNTX-I analogues determined by whole-cell patch clamp *.

Peptide	Amino Acid Sequence	$hNa_V1.7$ IC_{50} (μM)
Native HNTX-I	ECKGFGKSCVPGKNECCSGYACNSRDKWCKVLL	>10
E1G	**G**CKGFGKSCVPGKNECCSGYACNSRDKWCKVLL	>10
N23S	ECKGFGKSCVPGKNECCSGYAC**S**SRDKWCKVLL	0.435 ± 0.072
D26H	ECKGFGKSCVPGKNECCSGYACNSR**H**KWCKVLL	1.498 ± 0.093
L32W	ECKGFGKSCVPGKNECCSGYACNSRDKWCKV**W**L	>10
N23S–D26H	ECKGFGKSCVPGKNECCSGYAC**S**SR**H**KWCKVLL	0.079 ± 0.004
E1G–N23S–D26H	**G**CKGFGKSCVPGKNECCSGYAC**S**SR**H**KWCKVLL	0.179 ± 0.024
E1G–R25K–D26H	**G**CKGFGKSCVPGKNECCSGYACNS**KH**KWCKVLL	0.766 ± 0.029
N23S–D26H–L32W	ECKGFGKSCVPGKNECCSGYAC**S**SR**H**KWCKV**W**L	0.071 ± 0.005
E1G–R25K–D26H–L32W	**G**CKGFGKSCVPGKNECCSGYACNS**KH**KWCKV**W**L	0.669 ± 0.070
E1G–N23S–D26H–L32W	**G**CKGFGKSCVPGKNECCSGYAC**S**SR**H**KWCKV**W**L	0.036 ± 0.007

*—Data are presented as mean ± SEM, $n \geq 3$. Amino acid residues in red color represented the mutated residues.

2.3. Structure–Activity Relationship of HNTX-I and Mutant

We have added the NMR solution structure of HNTX-I to the Protein Data Bank (Figure 3A; PDB code 1NIX; www.rcbs.org/pdb). In HNTX-I's structure, the basic residues Arg25, Lys27 and Lys30 clustered to form a positively charged surface and interacted with VGSCs by electrostatic interaction. The vicinal hydrophobic residues Phe5, Tyr20, Trp28, Val31, Leu32 and Leu33 clustered to form a hydrophobic patch. Both the hydrophobic and the positively charged residues are highly conserved in NaSpTx family 1. We modeled the 3-D structure of E1G–N23S–D26H–L32W using that of HNTX-I as a template (Figure 3B). After we mutated acidic residue Asp26 to basic residue His26, the intensity of the electrostatic interaction of the original positively charged surface was enhanced. In addition, Gly1 reduced the negative charge. All these factors may affect the electrostatic properties of the peptide and change its pharmacological specificity. Furthermore, the aromatic group Trp32 strengthened

hydrophobic interaction in the hydrophobic patch, and S23 was required to orient the critical Trp29 and Lys31 residues correctly [20,26]. Taken together, these results suggest that in addition to the highly conserved charged surface and the hydrophobic surface, less-conserved acidic residues and surrounding residues play important roles in pharmacological flexibility.

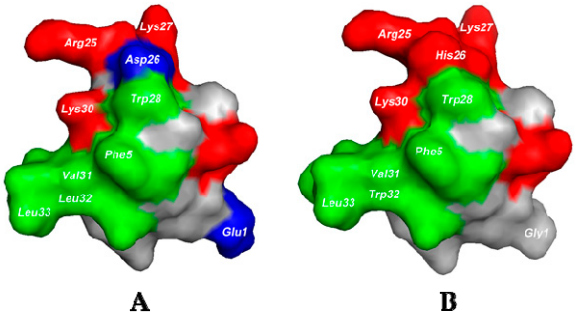

Figure 3. Surface rendering of NMR structure of HNTX-I and HNTX-I analogue E1G–N23S–D26H–L32W. (**A**) Surface rendering of HNTX-I (PDB code 1NIX); (**B**) Surface rendering of a homology model of HNTX-I analogue E1G–N23S–D26H–L32W. Positively charged residues are shown in red, negatively charged residues in blue, hydrophobic residues in green, and polar uncharged residues in gray. This figure was generated using PyMOL.

3. Discussion

The VGSC $Na_V1.7$ is preferentially expressed in peripheral sensory neurons. Genetic, preclinical animal models and functional studies have shown that $Na_V1.7$ regulates sensory-neuron excitability and is a major contributor to several sensory modalities [27]. Because of the key role of $Na_V1.7$ in the nervous system, it is a hot target for the action of peptide toxins derived from defensive or predatory animal venoms such as HWTX-IV, HNTX-IV and μ-SLPTX-Ssm6a. These toxins have exhibited remarkable analgesia in several animal models [28–30]. Therefore, the $hNa_V1.7$ channel is considered an analgesic target and is the focus of drug design. Peptide toxins inhibiting $Na_V1.7$ activation are remarkably similar; they trap the voltage sensor of domain II s3b-s4, which is a hot-paddle motif in $Na_V1.7$ [31,32]. The mutations in s3b-s4 significantly disrupt the binding of toxins, especially charged amino acids D816 and E818 located in domain II s3b-s4 [32,33]. This evidence suggests that peptide toxins inhibit $Na_V1.7$ by use of conventional approaches and that similar activity domains may exist on peptide toxins.

In this study, we engineered HNTX-I and explored its analogues' inhibitory activity against established pain target $hNa_V1.7$. Recently, the $X_1X_2SWCKX_3$ motif, in which X stands for any hydrophobic residues and S is required to position W and K correctly, was proposed to be essential for the activity of peptides on $Na_V1.7$ [26]. In our study, the gain-of-function analogue E1G–N23S–D26H–L32W achieved high potency against $Na_V1.7$ with an IC_{50} value of 0.036 ± 0.007 μM, and its structure pattern conformed to the proposed motif. E1G–N23S–D26H–L32W also exhibited inhibitory activity on $Na_v1.2$ and $Na_v1.6$ channels (Figure S3), and further studies are required to optimize Na_v subtype selectivity for potential therapeutic use. Residue in position 26 was not conserved as well as it was in positions 1 and 32. These variable residues may determine pharmacological specificity against insect or mammalian VGSCs. His26 clustering with Arg25, Lys27 and Lys30 formed the charged surface, and Trp32 together with surrounding residues Phe5, Tyr20, Trp28, Val31 and Leu33 combined to form the hydrophobic surface. These surfaces together determined and modified the peptide's binding affinity to the $Na_V1.7$ channel. Moreover, these key residues together with the $X_1X_2SWCKX_3$ motif can be used as an important scaffold when designing or modifying peptides with structure patterns similar to that of the NaSpTx family 1 in the future. Engineering peptides based on sequence and structure conservation in the family appears to be a more economical and efficient way than positional scanning with representative members of different

classes of amino acids. The strategy of combining structure–activity relationships and the conservation of sequence evolution will together provide better insight into peptide drug design.

4. Materials and Methods

4.1. Peptide Synthesis, Oxidative Folding, Purification and Characterization

We synthesized HNTX-I analogues using a fluorenylmethyloxycarbonyl protecting group (Fmoc; *N*-(9-Fluorenyl)methoxycarbonyl)/tert-butyl strategy and a coupling method involving 1-hydroxy-benzotriazole (HOBt), *O*-(benzotriazol-1-yl)-1,13,3-tetramethyluronium hexafluorophosphate (TBTU) and *N*-methylmorpholine (NMM) [34]. We then purified the linear peptides by semi-preparative reverse-phase high-performance liquid-chromatography (RP-HPLC) purification (C_{18} column, 10 mm × 250 mm; Welch Materials Inc., Shanghai, China) with a 20-min linear acetonitrile gradient of 20–40% at a 3 mL/min flow rate (Hanbon HPLC system equipped with NP7000 serials pump and NU3000 serials UV/VIS detector, Hanbon Science & Technology Co., Ltd., Huai'an, China). The refolding buffer contained (in mM): 100 NaCl, 5 glutathione (GSH), 0.5 glutathione disulfide (GSSG) and 100 Tris (pH = 8.0, adjusted with NaOH). We diluted the purified linear peptide with the refolding buffer to a final concentration of 0.1 mg/mL, slowly stirred the solution at 25 °C for 24 h, and monitored the refolding reaction by matrix-assisted laser desorption/ionization (MALDI)–time–of–flight (TOF) mass spectrometry (MS) analysis (AB SCIEX TOF/TOF^{TM} 5800 system; Applied Biosystems, Foster City, CA, USA). We terminated the reaction by adding trifluoroacetic acid (TFA) to a final concentration of 0.2% and isolated the desired oxidized peptide by RP-HPLC purification (C_{18} column, 4.6 mm × 250 mm; Welch Materials, Inc., Shanghai, China) using a 20-min linear acetonitrile gradient of 20–40% at a 1 mL/min flow rate (Hanbon HPLC system equipped with NP7000 serials pump and NU3000 serials UV/VIS detector; Hanbon Science & Technology Co., Ltd., Huai'an, China). The synthesis and oxidative folding of wild-type HNTX-I and E1G-N23S-D26H-L32W were shown in Supplementary Materials.

4.2. Cell Culture and Transfection

We maintained human embryonic kidney (HEK) 293 cells at 37 °C in a humidified 5% CO_2 incubator in Dulbecco's Modified Eagle's Medium (DMEM) supplemented with 10% fetal bovine serum (FBS), 2 mM L-glutamine, 100 units/mL penicillin and 100 μg/mL streptomycin. cDNA genes encoding rat $Na_v1.2$ and mouse $Na_v1.6$ were subcloned into the vectors pcDNA3.1, respectively. We subcloned the gene that encodes $hNa_V1.7$ into the vector pcDNA3.1-mod [35]. We transfected the $hNa_V1.7$ channel (3 μg) together with plasmids β1- (1 μg) and β2-eGFP (1 vg), which encode the human β1 and β2 subunits, and $Na_v1.2$ and $Na_v1.6$ together with eGFP in HEK 293 cells using Lipofectamine 2000 (Invitrogen, Carlsbad, CA, USA) per the manufacturer's instructions.

4.3. Whole-Cell Patch Clamp Recordings

We performed whole-cell recordings using an EPC 10 patch clamp platform (HEKA, Elektronik, Lambrecht, Germany) at room temperature (20–25 °C). We made suction pipettes with access resistance of 2.0–3.0 MΩ from borosilicate glass capillary tubes (VWR micropipettes; VWR Co., West Chester, PA, USA) using a 2-step vertical microelectrode puller (PC-10; Narishige Co., Ltd., Tokyo, Japan) and compensated for voltage errors using 80% serial-resistance compensation. The standard pipette solution contained (in mM): 140 CsCl, 10 NaCl, 1 ethylene glycol-bis (β-aminoethyl ether)-*N*,*N*,*N*′,*N*′-tetraacetic acid (EGTA), and 10 HEPES (pH 7.4). The bath solution contained (in mM): 140 NaCl, 2 $CaCl_2$, 1 $MgCl_2$, 5 KCl, 20 4-(2-hydroxyethyl)-1-piperazineethanesulfonic acid (HEPES) and 10 glucose (pH 7.4). We purchased all chemicals from Sigma-Aldrich (St. Louis, MO, USA) and dissolved them in water. Data were acquired using PATCHMASTER software version 2x73 (HEKA Elektronik Dr. Schulze GmbH, Lambrecht, Germany). We filtered macroscopic sodium currents at 5 kHz and sampled them at 20 kHz. We acquired voltage clamp recordings 5 min after establishing a

whole-cell configuration to allow adequate equilibration between the micropipette solution and the cell interior. We elicited channel current by 50 milliseconds of depolarization potential to −10 mV from the holding voltage of −100 mV.

4.4. Molecular Model of E1G-N23S-D26H-L32W

We modeled the 3-dimensional structure of E1G–N23S–D26H–L32W using the nuclear magnetic resonance (NMR)–derived structure of HNTX-I (PBD code 1NIX) as a template [36]. We performed backbone fitting and energy minimization using the Swiss Model prediction algorithm (open source; http://swissmodel.expasy.org) [37] and displayed them with PyMOL Molecular Graphics System software version 1.7.2 (Schrödinger, LLC, New York, NY, USA). The model was validated by inspection of the Ramachandran plot.

4.5. Data Analysis

We analyzed the data using Igor Pro software version 6.10A (WaveMetrics, Lake Oswego, OR, USA), Sigmaplot software version 10 (Sigma, St. Louis, MO, USA), OriginPro software version 8 (OriginLab Corp., Northampton, MA, USA) and Prism software version 5 (GraphPad Software, San Diego, CA, USA). Concentration–response curves were fitted using the following Hill logistic equation:

$$y = f_{max} - (f_{max} - f_{min})/(1 + (x/\mathrm{IC}_{50})^n) \quad (1)$$

where f_{max} and f_{min} respectively represent the channel's maximum and minimum responses to toxins, f_{min} was set to 0, x represents toxin concentration and n is an empirical Hill coefficient. All quantitative results are presented as mean ± standard error of the mean (SEM).

Supplementary Materials: The following are available online at http://www.mdpi.com/2072-6651/10/9/358/s1, Figure S1: Synthesis and oxidative folding of wild type HNTX-I, Figure S2: Synthesis and oxidative folding of HNTX-I analogue E1G-N23S-D26H-L32W, Figure S3: Effect of E1G-N23S-D26H-L32W on $Na_v1.2$ and $Na_v1.6$ expressed in HEK 293 cells.

Author Contributions: Z.L., X.Z. and Y.Z., conceived and designed the experiments; Y.Z., Q.Y., Q.Z., D.P. and M.C. performed the experiments; Z.L., X.Z., Y.Z. and S.L. analyzed the data; X.Z. and Y.Z. wrote the paper.

Funding: This work was funded by National Nature Science Foundation project of China (grant Nos. 31570782 and 31370817), and China Postdoctoral Science Foundation funded project (grant Nos. 2018M632968).

Conflicts of Interest: The authors declare no conflict of interest.

References

1. Gaskin, D.J.; Richard, P. The economic costs of pain in the United States. *J. Pain* **2012**, *13*, 715–724. [CrossRef] [PubMed]
2. Groenewald, C.B.; Essner, B.S.; Wright, D.; Fesinmeyer, M.D.; Palermo, T.M. The economic costs of chronic pain among a cohort of treatment-seeking adolescents in the United States. *J. Pain* **2014**, *15*, 925–933. [CrossRef] [PubMed]
3. Montgomery, W.; Sato, M.; Nagasaka, Y.; Vietri, J. The economic and humanistic costs of chronic lower back pain in Japan. *Clinicoecon. Outcomes Res.* **2017**, *9*, 361–371. [CrossRef] [PubMed]
4. Nightingale, S. The neuropathic pain market. Nature reviews. *Drug Discov.* **2012**, *11*, 101–102. [CrossRef] [PubMed]
5. Dworkin, R.H.; Panarites, C.J.; Armstrong, E.P.; Malone, D.C.; Pham, S.V. Is treatment of postherpetic neuralgia in the community consistent with evidence-based recommendations? *Pain* **2012**, *153*, 869–875. [CrossRef] [PubMed]
6. Torrance, N.; Ferguson, J.A.; Afolabi, E.; Bennett, M.I.; Serpell, M.G.; Dunn, K.M.; Smith, B.H. Neuropathic pain in the community: More under-treated than refractory? *Pain* **2013**, *154*, 690–699. [CrossRef] [PubMed]
7. Holmes, D. The pain drain. *Nature* **2016**, *535*, S2. [CrossRef] [PubMed]
8. Vetter, I.; Deuis, J.R.; Mueller, A.; Israel, M.R.; Starobova, H.; Zhang, A.; Rash, L.D.; Mobli, M. $Na_v1.7$ as a pain target—from gene to pharmacology. *Pharmacol. Ther.* **2017**, *172*, 73–100. [CrossRef] [PubMed]

9. Yang, Y.; Mis, M.A.; Estacion, M.; Dib-Hajj, S.D.; Waxman, S.G. $Na_v1.7$ as a pharmacogenomic target for pain: Moving toward precision medicine. *Trends Pharmacol. Sci.* **2018**, *39*, 258–275. [CrossRef] [PubMed]
10. Dib-Hajj, S.D.; Geha, P.; Waxman, S.G. Sodium channels in pain disorders: Pathophysiology and prospects for treatment. *Pain* **2017**, *158* (Suppl. 1), S97–S107. [CrossRef] [PubMed]
11. Yang, Y.; Huang, J.; Mis, M.A.; Estacion, M.; Macala, L.; Shah, P.; Schulman, B.R.; Horton, D.B.; Dib-Hajj, S.D.; Waxman, S.G. $Na_v1.7$-A1632G mutation from a family with inherited erythromelalgia: Enhanced firing of dorsal root ganglia neurons evoked by thermal stimuli. *J. Neurosci.* **2016**, *36*, 7511–7522. [CrossRef] [PubMed]
12. Eberhardt, M.; Nakajima, J.; Klinger, A.B.; Neacsu, C.; Huhne, K.; O'Reilly, A.O.; Kist, A.M.; Lampe, A.K.; Fischer, K.; Gibson, J.; et al. Inherited pain: Sodium channel $Na_v1.7$ A1632T mutation causes erythromelalgia due to a shift of fast inactivation. *J. Biol. Chem.* **2014**, *289*, 1971–1980. [CrossRef] [PubMed]
13. Wu, B.; Zhang, Y.; Tang, H.; Yang, M.; Long, H.; Shi, G.; Tang, J.; Shi, X. A novel scn9a mutation (F826Y) in primary erythromelalgia alters the excitability of $Na_v1.7$. *Curr. Mol. Med.* **2017**, *17*, 450–457. [CrossRef] [PubMed]
14. Imai, N.; Miyake, N.; Saito, Y.; Kobayashi, E.; Ikawa, M.; Manaka, S.; Shiina, M.; Ogata, K.; Matsumoto, N. Short-lasting unilateral neuralgiform headache attacks with ispilateral facial flushing is a new variant of paroxysmal extreme pain disorder. *J. Headache Pain* **2015**, *16*, 35. [CrossRef] [PubMed]
15. Suter, M.R.; Bhuiyan, Z.A.; Laedermann, C.J.; Kuntzer, T.; Schaller, M.; Stauffacher, M.W.; Roulet, E.; Abriel, H.; Decosterd, I.; Wider, C. p.L1612P, a novel voltage-gated sodium channel $Na_v1.7$ mutation inducing a cold sensitive paroxysmal extreme pain disorder. *Anesthesiology* **2015**, *122*, 414–423. [CrossRef] [PubMed]
16. Faber, C.G.; Hoeijmakers, J.G.; Ahn, H.S.; Cheng, X.; Han, C.; Choi, J.S.; Estacion, M.; Lauria, G.; Vanhoutte, E.K.; Gerrits, M.M.; et al. Gain of function $Na_v1.7$ mutations in idiopathic small fiber neuropathy. *Ann. Neurol.* **2012**, *71*, 26–39. [CrossRef] [PubMed]
17. Mansouri, M.; Chafai Elalaoui, S.; Ouled Amar Bencheikh, B.; El Alloussi, M.; Dion, P.A.; Sefiani, A.; Rouleau, G.A. A novel nonsense mutation in *SCN9A* in a moroccan child with congenital insensitivity to pain. *Pediatr. Neurol.* **2014**, *51*, 741–744. [CrossRef] [PubMed]
18. Emery, E.C.; Luiz, A.P.; Wood, J.N. $Na_v1.7$ and other voltage-gated sodium channels as drug targets for pain relief. *Expert Opin. Ther. Tar.* **2016**, *20*, 975–983. [CrossRef] [PubMed]
19. Vetter, I.; Davis, J.L.; Rash, L.D.; Anangi, R.; Mobli, M.; Alewood, P.F.; Lewis, R.J.; King, G.F. Venomics: A new paradigm for natural products-based drug discovery. *Amino Acids* **2011**, *40*, 15–28. [CrossRef] [PubMed]
20. Li, D.; Xiao, Y.; Hu, W.; Xie, J.; Bosmans, F.; Tytgat, J.; Liang, S. Function and solution structure of Hainantoxin-I, a novel insect sodium channel inhibitor from the chinese bird spider selenocosmia hainana. *FEBS Lett.* **2003**, *555*, 616–622. [CrossRef]
21. Saez, N.J.; Senff, S.; Jensen, J.E.; Er, S.Y.; Herzig, V.; Rash, L.D.; King, G.F. Spider-venom peptides as therapeutics. *Toxins* **2010**, *2*, 2851–2871. [CrossRef] [PubMed]
22. Klint, J.K.; Chin, Y.K.; Mobli, M. Rational engineering defines a molecular switch that is essential for activity of spider-venom peptides against the analgesics target $Na_v1.7$. *Mol. Pharmacol.* **2015**, *88*, 1002–1010. [CrossRef] [PubMed]
23. Murray, J.K.; Ligutti, J.; Liu, D.; Zou, A.; Poppe, L.; Li, H.; Andrews, K.L.; Moyer, B.D.; McDonough, S.I.; Favreau, P.; et al. Engineering potent and selective analogues of GpTx-1, a tarantula venom peptide antagonist of the Na(v)1.7 sodium channel. *J. Med. Chem.* **2015**, *58*, 2299–2314. [CrossRef] [PubMed]
24. Revell, J.D.; Lund, P.E.; Linley, J.E.; Metcalfe, J.; Burmeister, N.; Sridharan, S.; Jones, C.; Jermutus, L.; Bednarek, M.A. Potency optimization of Huwentoxin-IV on $hNa_v1.7$: A neurotoxin TTX-S sodium-channel antagonist from the venom of the Chinese bird-eating spider selenocosmia huwena. *Peptides* **2013**, *44*, 40–46. [CrossRef] [PubMed]
25. Shcherbatko, A.; Rossi, A.; Foletti, D.; Zhu, G.; Bogin, O.; Galindo Casas, M.; Rickert, M.; Hasa-Moreno, A.; Bartsevich, V.; Crameri, A.; et al. Engineering highly potent and selective microproteins against $Na_v1.7$ sodium channel for treatment of pain. *J. Biol. Chem.* **2016**, *291*, 13974–13986. [CrossRef] [PubMed]
26. Zhang, A.H.; Sharma, G.; Undheim, E.A.B.; Jia, X.; Mobli, M. A complicated complex: Ion channels, voltage sensing, cell membranes and peptide inhibitors. *Neurosci. Lett.* **2018**, *679*, 35–47. [CrossRef] [PubMed]
27. Dib-Hajj, S.D.; Yang, Y.; Black, J.A.; Waxman, S.G. The $Na_v1.7$ sodium channel: From molecule to man. *Nat. Rev. Neurosci.* **2013**, *14*, 49–62. [CrossRef] [PubMed]

28. Liu, Y.; Wu, Z.; Tang, D.; Xun, X.; Liu, L.; Li, X.; Nie, D.; Xiang, Y.; Yi, J.; Yi, J. Analgesic effects of Huwentoxin-IV on animal models of inflammatory and neuropathic pain. *Protein Peptide Lett.* **2014**, *21*, 153–158. [CrossRef]
29. Liu, Y.; Tang, J.; Zhang, Y.; Xun, X.; Tang, D.; Peng, D.; Yi, J.; Liu, Z.; Shi, X. Synthesis and analgesic effects of μ-TRTX-Hhn1b on models of inflammatory and neuropathic pain. *Toxins* **2014**, *6*, 2363–2378. [CrossRef] [PubMed]
30. Yang, S.; Xiao, Y.; Kang, D.; Liu, J.; Li, Y.; Undheim, E.A.; Klint, J.K.; Rong, M.; Lai, R.; King, G.F. Discovery of a selective $Na_v1.7$ inhibitor from centipede venom with analgesic efficacy exceeding morphine in rodent pain models. *Proc. Natl. Acad. Sci. USA* **2013**, *110*, 17534–17539. [CrossRef] [PubMed]
31. Bosmans, F.; Martin-Eauclaire, M.F.; Swartz, K.J. Deconstructing voltage sensor function and pharmacology in sodium channels. *Nature* **2008**, *456*, 202–208. [CrossRef] [PubMed]
32. Xiao, Y.; Bingham, J.P.; Zhu, W.; Moczydlowski, E.; Liang, S.; Cummins, T.R. Tarantula Huwentoxin-IV inhibits neuronal sodium channels by binding to receptor site 4 and trapping the domain II voltage sensor in the closed configuration. *J. Biol. Chem.* **2008**, *283*, 27300–27313. [CrossRef] [PubMed]
33. Liu, Z.; Cai, T.; Zhu, Q.; Deng, M.; Li, J.; Zhou, X.; Zhang, F.; Li, D.; Li, J.; Liu, Y.; et al. Structure and function of Hainantoxin-III, a selective antagonist of neuronal tetrodotoxin-sensitive voltage-gated sodium channels isolated from the Chinese bird spider Ornithoctonus hainana. *J. Biol. Chem.* **2013**, *288*, 20392–20403. [CrossRef] [PubMed]
34. Pi, J.; Quan, M.; Zeng, X. Solid-phase chemical synthesis and oxidative refolding of Hainantoxin-III. *Chin. J. Chromatogr.* **2007**, *25*, 399–403. [CrossRef]
35. Klugbauer, N.; Lacinova, L.; Flockerzi, V.; Hofmann, F. Structure and functional expression of a new member of the tetrodotoxin-sensitive voltage-activated sodium channel family from human neuroendocrine cells. *EMBO J.* **1995**, *14*, 1084–1090. [PubMed]
36. Gui, J.; Liu, B.; Cao, G.; Lipchik, A.M.; Perez, M.; Dekan, Z.; Mobli, M.; Daly, N.L.; Alewood, P.F.; Parker, L.L.; et al. A tarantula-venom peptide antagonizes the TRPA1 nociceptor ion channel by binding to the S1-S4 gating domain. *Curr. Biol.* **2014**, *24*, 473–483. [CrossRef] [PubMed]
37. Arnold, K.; Bordoli, L.; Kopp, J.; Schwede, T. The SWISS-MODEL workspace: A web-based environment for protein structure homology modelling. *Bioinformatics* **2006**, *22*, 195–201. [CrossRef] [PubMed]